Experimental Study of SO_2 Formation in the Reactions of CH_3SO Radical with NO_2 and O_3 in Relation with the Atmospheric Oxidation Mechanism of Dimethyl Sulfide

Dmitri Borissenko, Alexander Kukui,* Gérard Laverdet, and Georges Le Bras

Laboratoire de Combustion et Systèmes Réactifs, C.N.R.S., 1c av. de la Recherche Scientifique, 45071 Orléans Cedex 2, France

Received: July 22, 2002; In Final Form: November 19, 2002

Reactions of CH_3SO radicals with O_3 and NO_2 have been studied at 140−660 Torr pressure of N_2 and 300 K using the pulsed laser photolysis technique with direct monitoring of SO_2 formation by laser induced fluorescence with excitation at 220.6 nm. The yield of SO_2 in the reaction of CH_3SO with NO_2 has been found to be pressure dependent varying from (0.4 ± 0.12) at 100 Torr to (0.25 ± 0.05) at 664 Torr of N_2. This result is in agreement with our previous data obtained using different experimental approach and may be interpreted by the formation of activated CH_3SO_2* radical followed by its prompt decomposition or collisional stabilization. The SO_2 yield in the reaction of CH_3SO with O_3 has been found to be a factor (4.0 ± 0.3) higher than in the reaction with NO_2 corresponding to a yield of (1.0 ± 0.12) at 660 Torr of N_2. The rate constant for the reactions $CH_3SO + O_3$, $O + CH_3SSCH_3$, and $O + CS_2$ at 300 K have been found to be $(3.2 \pm 0.9) \times 10^{-13}$, $(1.06 \pm 0.07) \times 10^{-10}$, and $(3.6 \pm 0.1) \times 10^{-12}$ cm^3 molecule^{-1} s^{-1}, respectively. The implications of the obtained results to the SO_2 yield in the atmospheric oxidation of dimethyl sulfide (DMS) are discussed. The results suggest that the CH_3SO+O_3 reaction is a significant source of SO_2 in the mechanism of the DMS oxidation in the remote troposphere.

Introduction

Dimethyl sulfide (DMS), CH_3SCH_3, is the largest natural contributor to sulfur in the troposphere,[1] and its atmospheric oxidation has been suggested to play an important role in the formation of clouds by producing new sulfate particles which act as cloud condensation nuclei (CCN).[2] This source of non sea salt sulfate is considered to be predominantly the gas-phase oxidation of SO_2 to H_2SO_4 by reaction with OH. However, the quantitative mechanism of SO_2 formation by DMS oxidation and the variability of this SO_2 source efficiency with changing of atmospheric conditions remain poorly understood. The main initiation step of DMS oxidation is the reaction with OH, which proceeds by both abstraction and addition channels, the latter being dominant at low temperatures.[3,4] On the basis of the laboratory kinetic and end product analysis studies, it has been postulated that the key intermediates of the abstraction initiated oxidation pathway are CH_3SO_x ($x = 0,1,2,3$) radicals.[5,6] The principal mechanism of SO_2 formation has been suggested to include a sequence of reactions of CH_3SO_x radicals with O_2, NO_2, and O_3 as well as the thermal decomposition of CH_3SO_2.[5,6] The reactions of CH_3S with O_2,[7,8] O_3,[9−12] and NO_2[7,11,13−16] have been studied by several groups and the overall rate constants for these reactions seem to be well determined, although some discrepancies still remain.[16] The reactions of CH_3SO with O_3 and NO_2 have been studied less extensively. Dominé et al.[10,14] estimated the overall rate constants for the reactions of CH_3SO with NO_2 and O_3 using the low pressure (∼1−2 Torr) flow reactor techniques. Some conclusions have been drawn in these studies about the mechanism of these reactions, although the major channels have not been identified.

In our recent work,[17] the mechanism of the CH_3SO reaction with NO_2 has been studied by laser pulsed photolysis/LIF and discharge flow mass spectrometry/LIF techniques. On the basis of the analysis of the kinetics of CH_3O radical indirectly formed in the photolysis system and on ab initio and RRKM calculations, the reaction has been suggested to proceed via formation of chemically activated CH_3SO_2* radical followed by its prompt decomposition to CH_3 and SO_2 or thermal stabilization:

$$CH_3SO + NO_2 \rightarrow CH_3 + SO_2 + NO \quad (1a)$$

$$\rightarrow CH_3SO_2 + NO \quad (1b)$$

The branching ratio for the SO_2 formation (1a) has been found to be pressure and temperature dependent with a value $\alpha = k_{1a}/k_1 = (0.18 \pm 0.03)$ at 612 Torr of He and 300 K.

The reaction of CH_3SO radical with ozone is expected to be the major oxidation pathway for the CH_3SO radical under atmospheric conditions of a remote marine atmosphere where the SO_2/aerosol formation from DMS is an important issue. If the mechanisms of CH_3SO reactions with NO_2 and O_3 are similar, the yield of SO_2 in the reaction with ozone may be higher than in the reaction with NO_2 because of the higher enthalpy of the reaction 2 by about 48 kcal/mol:[17]

$$CH_3SO + O_3 \rightarrow CH_3 + SO_2 + O_2 \quad (2a)$$

$$\rightarrow CH_3SO_2 + O_2 \quad (2b)$$

In this work, we used direct detection of SO_2 by LIF to confirm our previous results on the mechanism of the reaction 1 and to determine the SO_2 yield in the reaction of CH_3SO with ozone.

Experimental Section

To quantify the SO_2 formation in the reaction of CH_3SO with ozone the yield of SO_2 in this reaction was compared with that in the reaction of CH_3SO with NO_2. Namely, the dependence of SO_2 yield on the ratio of $[O_3]$ to $[NO_2]$ was measured using

* To whom correspondence should be addressed. E-mail: kukuy@cnrs-orleans.fr.

10.1021/jp021701g CCC: $25.00
Published on Web 01/31/2003

pulsed laser photolysis of $DMS/O_3/NO_2$ mixture at 248 nm. The yield of SO_2 in the reaction of CH_3SO with NO_2 has been measured previously in this laboratory,[17] and it has been remeasured in this work by direct monitoring of the SO_2 formation from the photolysis of $DMDS/NO_2$ mixtures quantified using photolysis of CS_2/NO_2 mixtures at 351 nm. It is effectively known that the SO_2 yield in this latter system is near unity (see below).

The experimental setup was similar to that previously described[17] with some modifications concerning mainly the detection of SO_2.

The reaction cell consisted of a jacketed 5 cm diameter Pyrex flow tube with 15 cm long orthogonal sidearms equipped with light baffles and quartz windows. The photolysis and probe beams were perpendicular to each other and to the flow direction. The delay time between the photolysis and probe laser shots was varied from 10 μs to 100 ms.

The photolysis was performed at 248 or 351 nm using a KrF or XeF Lambda Physik excimer laser operating at a 10 Hz pulse repetition rate. The pulse energy of the rectangular (4 mm × 9 mm) excitation laser beam was measured for every pulse with a pyroelectric detector and kept below 1 mJ cm^{-2} using a neutral density filter.

In previous studies from this laboratory,[17,18] the SO_2 was detected by LIF using fluorescence excitation at around 290 nm corresponding to the $\tilde{B}^1B_1,\tilde{A}^1A_2 \leftarrow \tilde{X}^1A_1$ electronic transition. Because of relatively long fluorescence lifetime, $\tau_f > 30$ μs, and fast fluorescence quenching[19] the measurements were possible only at low pressure ($P < 20$ Torr). In this study, SO_2 was detected using laser induced fluorescence of a $\tilde{C}^1B_2 - \tilde{X}^1A_1$ band. The relatively short fluorescence lifetime of the $\tilde{C}^1B_2$-(1,3,2) electronic state excited at 220.63 nm, $\tau_f \approx 40$ ns,[20] allows detection of SO_2 in the pressure range 100−660 Torr of N_2 used in this work. The fluorescence was excited using frequency doubled output of a Lambda Physik FL3002 tunable dye laser (Coumarine 120 dye) pumped by a Continuum Surelite I-10 Nd:YAG laser. The dye laser pulse energy was ∼100 μJ and was monitored after passing the fluorescence cell by a LAS PM200 pyroelectric detector for every pulse.

The emitted fluorescence was detected by a Hamamatsu R2560 photomultiplier after passing through a broadband filter (250−400 nm). The multiplier output was amplified with a fast preamplifier SRS D-300. The preamplifier output was connected to a Textronix TDS 3032 oscilloscope which was programmed to calculate an area under averaged over 128 laser pulses and exponentially decayed fluorescence signals with the integration gate of about 50 ns. Observed fluorescence decay times were about 10−20 ns depending on pressure. The measured signals had to be corrected for the contribution from excitation laser pulses and from background fluorescence which was significant in the presence of high concentrations of sulfur gases, such as CS_2 and dimethyl disulfide (DMDS) CH_3SSCH_3. This contribution was measured with a delay of about 90 ms after the photolysis laser pulse when all SO_2 produced in the photolysis initiated reactions had been removed from the detection zone by the gas flow. After background subtraction the SO_2 LIF signals were normalized to the photolysis and the probe laser pulse energies.

The fluorescence excitation spectra obtained from SO_2 added to a flow of N_2, as well as from the photolysis of reaction mixtures used in this study, were identical to the SO_2 absorption spectra from the literature,[21] as exemplified in Figure 1 for CS_2/NO_2 photolysis. Linear dependence of the LIF signal on the SO_2 concentration for $[SO_2] \approx 10^{10}-10^{14}$ molecule cm^{-3} has been verified by addition of known SO_2 concentrations into the cell in the presence of other reactants used in this study. The detection limit of the method corresponding to S/N = 1 was 10^8-10^{10} molecule cm^{-3} depending on pressure and background signal intensity, the latter being proportional to the concentration of sulfur compounds in the reaction cell. The influence of fluorescence quenching by the reactant gases on the sensitivity was negligible in the range of concentrations used in this study.

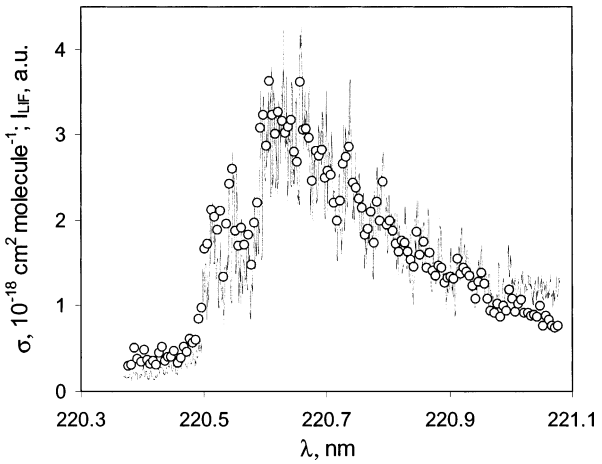

Figure 1. Fluorescence excitation spectrum of SO_2 obtained by photolysis of CS_2/NO_2 mixture at 351 nm (○) and literature SO_2 absorption spectrum[21] (−).

DMDS (Aldrich), DMS (Aldrich), and CS_2 (Aldrich) diluted in He after degassing (CS_2 was purified by trap-to-trap distillation and degassed at 77 K) were stored in 20 l glass bulbs and were added to the N_2 carrier gas flow in the glass manifold. The concentrations of DMDS, DMS, and CS_2 were measured prior to entrance to the fluorescence cell by absorption at 213.9 nm (zinc lamp, 214 nm band-pass filter) using independently measured in this work absorption cross sections of 2.8×10^{-18}, 1.7×10^{-18}, and 3.2×10^{-18} cm^2 $molecule^{-1}$, respectively. The DMS absorption cross section value is in agreement with literature data.[22] The DMDS and CS_2 values are different from the literature data ($\sigma_{DMDS} = 3.7 \times 10^{-18}$ cm^2 $molecule^{-1}$;[22] $\sigma_{CS2} = 3.6 \times 10^{-18}$ cm^2 $molecule^{-1}$ [23]) and represent rather experimental parameters of the absorption cells used in this work. Ozone was stored on silica gel at 196 K and was eluted from the trap with a measured flow of N_2. Concentration of ozone was measured in an absorption cell before the entrance to the reactor by absorption at 253.7 nm using a cross section of 1.15×10^{-17} cm^2 $molecule^{-1}$ [24]. NO_2 (Alphagaz 2) was purified in excess of O_2 and stored in 20 l darkened glass bulb after dilution (0.5−5% in He or N_2). The NO_2 concentration was determined by the rate of pressure change in a calibrated volume and was corrected to account for the NO_2 dimerization.

Experimental Results

Photolysis of $DMDS/NO_2$ and CS_2/NO_2 Mixtures. Generation of O atoms by the photolysis of NO_2 at 351 nm invokes a sequence of reactions leading to SO_2 formation in both $DMDS/NO_2$ and CS_2/NO_2 mixtures. The reaction scheme for the $DMDS/NO_2$ photolysis includes reactions 3−5 and 1:

$$NO_2 + h\nu\ (\lambda{=}351\ \text{nm}) \rightarrow O + NO \quad (3)$$

$$O + DMDS \rightarrow CH_3SO + CH_3S \quad (4)$$

$$CH_3S + NO_2 \rightarrow CH_3SO + NO \quad (5)$$

Typical example of the SO_2 formation from the $DMDS/NO_2$ photolysis is presented in Figure 2. The yield of SO_2 was measured at reaction times 2−4 ms, long enough for the

TABLE 1: Photolysis of DMDS/NO_2 and CS_2/NO_2: Experimental Conditions and Results

P, Torr	$k_4(\pm 2\sigma)$, 10^{-10} cm^3molecule^{-1} s^{-1}	$k_7(\pm 2\sigma)$, 10^{-12} cm^3molecule^{-1} s^{-1}	$\alpha = k_{1a}/k_1$ $(\pm 2\sigma)$	$[NO_2]$, 10^{15} molecule cm^{-3}	[DMDS], 10^{14} molecule cm^{-3}	$[CS_2]$, 10^{16} molecule cm^{-3}
102	0.90 ± 0.35	3.18 ± 0.25	0.40 ± 0.12	0.25−2.7	6	0.52
184	1.01 ± 0.24	3.78 ± 0.2	0.28 ± 0.04	0.476−4.1	8.7	0.48
246	0.91 ± 0.32	3.19 ± 0.28	0.34 ± 0.05	0.65−7.8	12	1.1
246	0.89 ± 0.17	3.32 ± 0.21	0.25 ± 0.05	0.53−3.0	0.33	1.1
311	1.18 ± 0.36	3.91 ± 0.45	0.27 ± 0.04	0.68−10	8.7	0.81
344	1.93 ± 0.36	4.02 ± 0.19	0.37 ± 0.09	0.735−12.2	13	1.0
397	1.46 ± 0.22	3.64 ± 0.3	0.26 ± 0.05	0.74−7.3	4.5	0.85
497	0.86 ± 0.15	3.84 ± 0.25	0.34 ± 0.08	0.58−12.5	4	1.4
539	1.21 ± 0.12	3.32 ± 0.24	0.23 ± 0.06	0.85−11	8	1.3
607	0.9 ± 0.23	3.36 ± 0.23	0.25 ± 0.05	0.61−7.5	3.6	0.68
664	0.76 ± 0.17	3.15 ± 0.49	0.25 ± 0.05	0.5−9	9	1
mean	1.06 ± 0.07	3.6 ± 0.1				

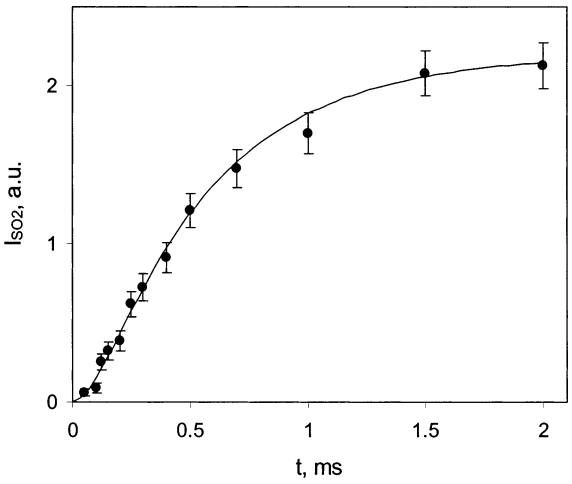

Figure 2. Kinetics of SO_2 formation in the photolysis of DMDS/NO_2: (●) experimental data at P = 176 Torr, [DMDS] = 1.54×10^{14} molecule cm^{-3}, $[NO_2] = 1.45 \times 10^{14}$ molecule cm^{-3}; solid line: calculated profile using $k_1 = 1.5 \times 10^{-11}$ cm^3 $molecule^{-1}$ s^{-1}.[17]

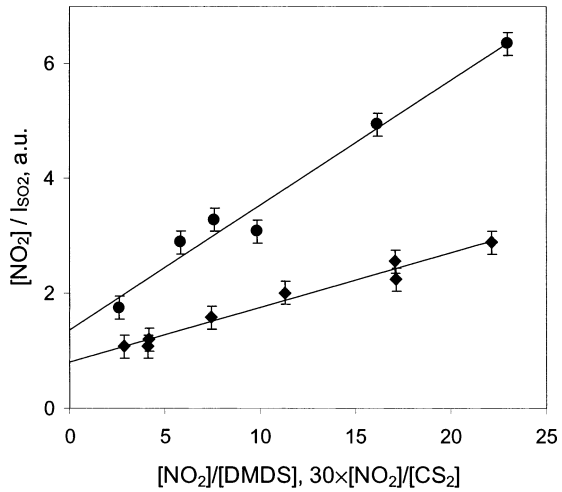

Figure 3. Comparison of SO_2 yields in the photolysis of DMDS/NO_2 (●) and CS_2/NO_2 (◆) at P = 607 Torr, [DMDS] = 3.6×10^{14} molecule cm^{-3}, $[CS_2] = 7 \times 10^{15}$ molecule cm^{-3}, and $[NO_2] = (0.61-7.5) \times 10^{15}$ molecule cm^{-3}.

complete formation of SO_2 in reaction 1a, but sufficiently short compared to thermal decomposition time of the CH_3SO_2 radical, (> 10 ms),[17] possibly formed in reaction 1b. As the conversion of O atoms into CH_3SO radicals in reactions 4[25] and 5[7,14] is about unity, the photolysis yield of SO_2 is determined by the SO_2 yield in the reaction 1a, $\alpha = k_{1a}/k_1$, and by the ratio of O atoms consumed in the reactions with DMDS (4) and NO_2 (6)

$$O + NO_2 \rightarrow NO + O_2 \qquad (6a)$$

$$O + NO_2 + M \rightarrow NO_3 + M \qquad (6b)$$

Neglecting quadratic reactions of O atoms, CH_3S, and CH_3SO radicals, the ratio of $[NO_2]$ to $[SO_2]$ formed in reaction 1a may be expressed as:

$$\frac{[NO_2]}{I_{SO_2}} = \frac{C}{2\alpha}\left(1 + \frac{k_6}{k_4}\frac{[NO_2]}{[DMDS]}\right) \qquad (I)$$

where I_{SO_2} is the SO_2 LIF signal and C is an instrumental constant. Equation I makes use of the proportionality of initial concentration of O atoms to the NO_2 concentration.

In the CS_2/NO_2 reference system, the O atoms react with CS_2 to form predominantly SO radicals[24] which are converted to SO_2 by fast reaction with NO_2:[24]

$$O + CS_2 \rightarrow CS + SO \qquad (7)$$

$$SO + NO_2 \rightarrow SO_2 + NO \qquad (8)$$

S atoms formed in the minor channel of the $O + CS_2$ reaction[26] are also converted to SO by fast reaction with NO_2.[27] Hence, the SO_2 yield in the CS_2/NO_2 photolysis with accounting for reaction 6 is close to unity and may be expressed as

$$\frac{[NO_2]}{I_{SO_2}} = C\left(1 + \frac{k_6}{k_7}\frac{[NO_2]}{[CS_2]}\right) \qquad (II)$$

where C is the same constant as in (I).

The dependences of $[NO_2]/I_{SO_2}$ ratios on $[NO_2]$/[DMDS] and $[NO_2]/[CS_2]$ ratios were obtained from the photolysis of DMDS/NO_2 and CS_2/NO_2, respectively, at different pressures by measuring the dependences of SO_2 LIF signal intensity on the NO_2 concentration (see Table 1). In agreement with equations I and II, the dependencies were found to be linear (see Figure 3). The ratios of slope to intercept of these dependences were used to calculate the ratios k_6/k_4 and k_6/k_7. The rate constants k_4 and k_7 reported in Table 1 were calculated using $k_{6a} = 1.07 \times 10^{-11}$ cm^3 $molecule^{-1}$ s^{-1} [28] and k_{6b} varying with pressure from 1.15×10^{-11} to 1.48×10^{-11} cm^3 $molecule^{-1}$ s^{-1} from 100 to 670 Torr.[29] The obtained $k_7 = (3.6 \pm 0.1) \times 10^{-12}$ cm^3 $molecule^{-1}$ s^{-1} is in good agreement with literature data $k_7 = 3.6 \times 10^{-12}$ cm^3 $molecule^{-1}$ s^{-1},[24] validating the experimental approach. The rate coefficient for the reaction O + DMDS has been previously measured two times with resulting values which differ by a factor of 2: 2.1×10^{-10} cm^3 $molecule^{-1}$ s^{-1} [30] and 1×10^{-10} cm^3 $molecule^{-1}$ s^{-1}.[31] The value

$$k_4 = (1.06 \pm 0.07) \times 10^{-10}\ cm^3\ molecule^{-1}\ s^{-1}$$

obtained in this work is very close to the value of Nip et al.[31]

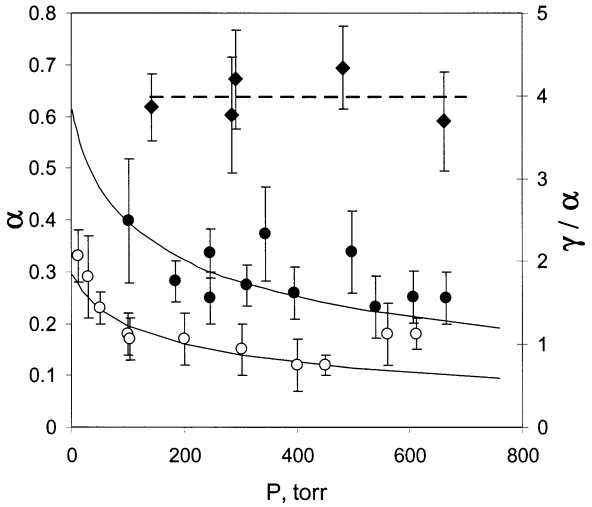

Figure 4. Pressure dependence of SO_2 yields in the reactions of CH_3SO with NO_2 (●) and with O_3 (◆). Open circles represent previous results obtained from the kinetics of CH_3O radicals.[17] Solid lines are results of ab initio and RRKM calculations[17] (see text).

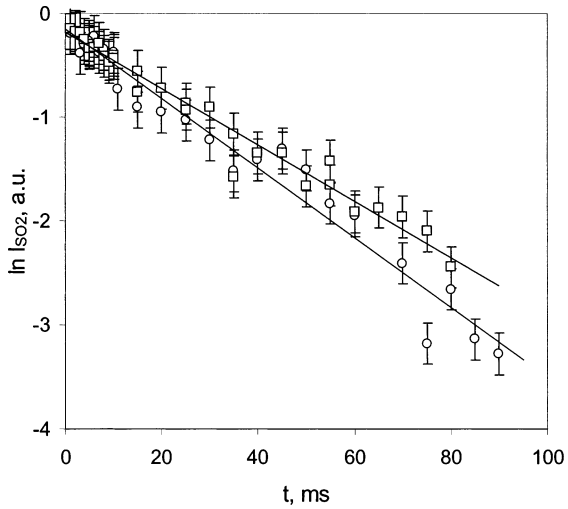

Figure 5. Comparison of the temporal decays of the LIF signal intensities of SO_2 in NO_2/DMDS (□) and NO_2/CS_2 (○) mixtures: P = 300 Torr, [DMDS] = 1.1×10^{14} molecule cm^{-3}, [CS_2] = 9.8×10^{15} molecule cm^{-3}, and [NO_2] = 3.6×10^{14} molecule cm^{-3}.

The yields of SO_2 in reaction 1a, α, at different pressures (Figure 4 and Table 1) were calculated from the ratio of intercepts of the linear dependences described by the expressions I and II and are exemplified in Figure 3. The obtained SO_2 yields depend on pressure decreasing from $\alpha = 0.4 \pm 0.1$ at 100 Torr to $\alpha = 0.25 \pm 0.05$ at 607 Torr.

Measurements of SO_2 signal intensity decay at long reaction time (up to 100 ms) using slow flow rates of N_2 carrier gas (Figure 5) and 1 Hz photolysis repetition rate show that the decay with the CS_2/NO_2 mixture is faster than that with the DMDS/NO_2 mixture. Although the decay under these conditions is mainly due to diffusional and convective removal of SO_2 out of the detection zone, the slower decay with the DMDS/NO_2 mixture can be explained by the SO_2 formation in the process of CH_3SO_2 thermal decomposition:

$$CH_3SO_2 + M \rightarrow CH_3 + SO_2 + M \qquad (9)$$

Neglecting the consumption of CH_3SO_2 in the reaction with NO_2 ($k_{CH_3SO_2+NO_2} < 1 \times 10^{-15}$ cm^3 molecule^{-1} s^{-1}),[17] the rate

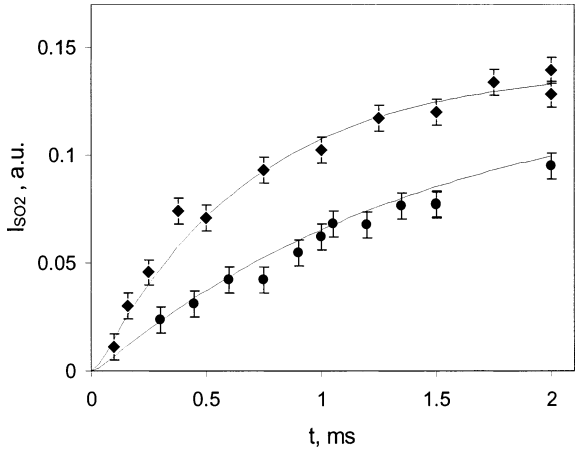

Figure 6. Kinetics of SO_2 formation in the photolysis of DMS/O_3 mixtures at P = 317 Torr, [DMS] = 8.13×10^{14} molecule cm^{-3} and different O_3 concentrations: (●) [O_3] = 1.56×10^{15} molecule cm^{-3}; (◆) [O_3] = 3.43×10^{15} molecule cm^{-3}. Solid lines: calculated profiles using $k_2 = 4.1 \times 10^{-13}$ cm^3 molecule^{-1} s^{-1}.

of the thermal decomposition (9) has been estimated to be lower than 1 s^{-1}

$$k_9(300\ \text{K}) \leq 1\ \text{s}^{-1}$$

This is consistent with our previous estimation $k_9 \leq 100$ s^{-1}.[17] Another possible explanation of the observed SO_2 formation at long reaction times with the DMDS/NO_2 mixture would be the regeneration of CH_3S or CH_3SO, which would also result in slow formation of SO_2 according to reactions 4 and 5. Accounting for this effect would lower the upper limit for the thermal decomposition rate of CH_3SO_2 at 300 K.

Photolysis of DMS/O_3/NO_2 Mixture. Formation of SO_2 in the reaction of CH_3SO with O_3 was studied using photolysis of DMS/O_3/NO_2 mixtures in N_2 bath gas at 248 nm. As shown in Figure 6 for a typical kinetics of SO_2 formation without NO_2, a rise of SO_2 LIF signal was followed by a stationary level and the time to reach this level was dependent on the ozone concentration. Assuming a simple mechanism of SO_2 formation according to a reactions sequence (10), (11),[24] and reaction of CH_3SO with O_3 (2)

$$O_3 + h\nu\ (\lambda{=}248\ \text{nm}) \rightarrow O + O_2 \qquad (10)$$

$$O + DMS \rightarrow CH_3SO + CH_3 \qquad (11)$$

the observed experimental SO_2 profiles could be described by a simulation using the reaction rate constants $k_2 = (3 \div 5) \times 10^{-13}$ cm^3 molecule^{-1} s^{-1} (see Figure 6).

In presence of NO_2, the SO_2 yield from the photolysis of DMS/O_3/NO_2 estimated by measuring the SO_2 LIF signal at long reaction times was dependent on the concentration of NO_2. The yield decreased with increasing [NO_2]. This dependence remained negative after correction for the partial consumption of O atoms by NO_2 in reaction 6. This dependence indicated a higher SO_2 yield in the reaction of CH_3SO with O_3 (2) than in the reaction of CH_3SO with NO_2 (1).

The branching ratio for SO_2 formation in reaction 2 $\gamma = k_{2a}/k_2$ was deduced from the dependence of SO_2 LIF signal I_{SO2} on the [O_3]/[NO_2] concentrations ratio using the values of $\alpha = k_{1a}/k_1$ derived in this work. The I_{SO2} was measured at reaction times 2−4 ms corresponding to the complete SO_2 formation. Assuming the reactions of CH_3SO with O_3 and NO_2 to be the major sources of SO_2, the following relation can be derived for

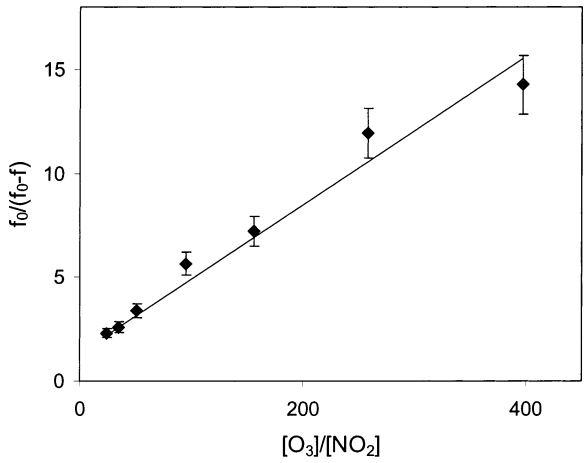

Figure 7. Dependence of the SO_2 yield (see text) in photolysis of $DMS/O_3/NO_2$ mixture on the $[O_3]/[NO_2]$ ratio at $P = 661$ Torr, $[DMS] = 4.2 \times 10^{14}$ molecule cm^{-3}, $[O_3] = 5.3 \times 10^{15}$ molecule cm^{-3}, and $[NO_2] = (0-2) \times 10^{14}$ molecule cm^{-3}.

the ratio of the formed SO_2 to the initial O atom concentration, $[SO_2]/[O]_0$:

$$\frac{[SO_2]}{[O]_0} = \frac{\gamma k_2[O_3] + \alpha k_1[NO_2]}{k_2[O_3] + k_1[NO_2]} \times \frac{k_{11}[DMS]}{k_{11}[DMS] + k_6[NO_2]} \quad \text{(III)}$$

Accounting that $[O]_0$ is proportional to the ozone concentration and introducing directly measurable quantities f and f_0

$$f = \frac{I_{SO_2}}{[O_3]} \times \left(1 + \frac{k_6[NO_2]}{k_{11}[DMS]}\right); f_0 = f_{[NO_2]=0} = \frac{I_{SO_2}}{[O_3]}$$

the relation (III) may be rewritten as follows:

$$\frac{f_0}{f_0 - f} = \frac{1}{1 - \alpha/\gamma} + \frac{1}{1 - \alpha/\gamma} \times \frac{k_2}{k_1} \frac{[O_3]}{[NO_2]} \quad \text{(IV)}$$

Experimental plots of $f_0/(f_0 - f)$ vs $[O_3]/[NO_2]$ (Figure 7) obtained by varying the NO_2 concentration at constant O_3 and DMS concentrations were found to be linear. Such linear plots obtained at several pressures were used to derive the ratios α/γ and k_2/k_1 as intercepts and ratios of slope to intercept, respectively. The results and experimental conditions of these experiments are presented in Table 2. Rate constant ratio k_2/k_1 was found to be independent of pressure with a mean value $k_2/k_1 = (2.13 \pm 0.13) \times 10^{-2}$. Using $k_1 = (1.5 \pm 0.4) \times 10^{-11}$ cm^3 $molecule^{-1}$ s^{-1} [17] we obtain

$$k_2 = (3.2 \pm 0.9) \times 10^{-13}\ cm^3\ molecule^{-1}\ s^{-1}$$

This value is within uncertainty limits of the only previous result of Dominé at al.[10] $k_2 = (6 \pm 3) \times 10^{-13}$ cm^3 $molecule^{-1}$ s^{-1}.

The ratio of the SO_2 yield in the reactions of CH_3SO with O_3 and NO_2, γ/α, does not exhibit apparent pressure dependence with a mean value

$$\gamma/\alpha = (4.0 \pm 0.3) \text{ at } P_{N2} = 140-660 \text{ Torr.}$$

Using the α values obtained in the present work this corresponds to a SO_2 yield of unity in reaction 2 at pressure $P_{N2} = 500-700$ Torr:

$$\gamma = k_{2a}/k_2 = (1.0 \pm 0.2) \text{ at } P_{N2} = 500-700 \text{ Torr.}$$

At lower pressures, the apparent SO_2 yield in reaction 2 increases with decreasing of pressure: $\gamma(500-100 \text{ Torr}) = 1-1.6$. This is possibly due to some radical branching reactions in photolyzed $DMS/O_3/NO_2$ mixtures (see discussion).

Discussion

The values of $\alpha = k_{1a}/k_1$ obtained in this work are somewhat higher than that reported earlier[17] (Figure 4), the difference being larger at lower pressures, about a factor of 2 at 100 Torr, and less significant at higher pressures where the difference is about 20% and close to the estimated accuracy of the experimental points. The previous results were obtained indirectly by comparing the CH_3O concentration profiles in the photolysis of $DMDS/NO_2$ and CH_3I/NO_2 mixtures and required using of several reaction rate constants with combined systematic error which could be rather large. In the present study, α was determined directly with the only assumption made being the reaction mechanism described by reactions 3−5 and 1. The validity of this mechanism has already been discussed in our previous work.[17] The accuracy of the present measurements was determined by the precision of the SO_2 LIF signal detection and by the accuracy of the DMDS, CS_2, and NO_2 concentrations measurements. The accuracy of the ratios k_6/k_4 and k_6/k_7 determination was controlled by the same factors. Hence, considering good agreement of the values $k_4 = (1.06 \pm 0.07) \times 10^{-10}$ and $k_7 = (3.6 \pm 0.1) \times 10^{-11}$ cm^3 $molecule^{-1}$ s^{-1} obtained in this work with the literature data,[24,31] we assume that there is no significant systematic error in the present measurements of α.

The dependence of α on pressure is similar to that obtained earlier and may be described with the mechanism of SO_2 formation in reaction 1a via decomposition of excited CH_3SO_2* radical using a decomposition energy of 14.69 kcal mol^{-1} obtained using G2 ab initio calculations[17] and an excess energy of 14.3 kcal mol^{-1}. This latter value is 0.6 kcal mol^{-1} higher than that providing the best fit to the data derived from the kinetics of CH_3O radicals in our previous work.[17] Both calculation results are presented in Figure 4.

The only previous study[10] of the mechanism of the CH_3SO reaction with O_3 has been performed at low pressure, 1−2 Torr of He. On the basis of the product analysis by photoionization mass spectrometry, the CH_3S forming channel has been quantified, $k_{2c}/k_2 = 13 \pm 6\%$.

$$CH_3SO + O_3 \rightarrow CH_3S + 2O_2 \quad \text{(2c)}$$

No other channels of the reaction 2 have been unambiguously identified, although observed kinetics indicated the occurrence of branched chain reactions and allowed to suggest that the major channel at low pressure may form an activated CH_3SO_2* product followed by its collisional stabilization (2b) or its decomposition according to (2a) and other possible decomposition channels.[10] This mechanism is consistent with our present data, indicating that the major channel of the reaction 2 at atmospheric pressure is channel 2a with formation of SO_2. According to our results, the yield of SO_2 at high pressure (500−700 Torr) is 100%, ($\gamma = 1.0 \pm 0.2$). That means that, if the reaction of CH_3SO with O_3, by analogy with the NO_2 reaction, proceeds via formation of the activated CH_3SO_2*, the collisional stabilization at atmospheric pressure is not efficient enough for its thermalization. The SO_2 yield higher than unity observed in our experiments at lower pressures (100−500 Torr) may be due to some branched regeneration of radicals similar to that observed in earlier studies of CH_3S/CH_3SO−ozone chemistry.[9−11] In the present study, this effect, if present, was significant only

TABLE 2: Photolysis of DMS/NO_2/O_3: Experimental Conditions and Results

P, Torr	$k_2/k_1(\pm 2\sigma)$, 10^{-2}	γ/α ($\pm 2\sigma$)	$[NO_2]$, 10^{14} molecule cm^{-3}	[DMS], 10^{14} molecule cm^{-3}	$[O_3]$, 10^{15} molecule cm^{-3}
142	2.17 ± 0.20	3.9 ± 0.4	0−1.7	1.6	5.2
285	1.79 ± 0.30	3.77 ± 0.7	0−2.7	0.8	5.5
292	1.97 ± 0.39	4.2 ± 0.6	0−21.0	9.2	11.0
481	2.35 ± 0.34	4.3 ± 0.5	0−3.7	2.1	7.0
661	2.27 ± 0.28	3.7 ± 0.6	0−2.2	4.2	5.3
mean	2.13 ± 0.13	4.0 ± 0.3			

at the lowest pressure, $P \approx 100$ Torr, used in this study. At higher pressure, the maximum apparent yield was close to unity, considering combined uncertainties on the values α and γ. Also, no indication of radicals regeneration leading to SO_2 production was found from the kinetics of SO_2 formation, as shown in Figure 6, where a good fit was obtained between the experimental kinetics and those calculated using the reaction mechanism (10), (11), and (2).

Formation of CH_3S radical in reaction 2c may lead to the formation of SO_2 via regeneration of CH_3SO in the reaction of CH_3S with O_3

$$CH_3S + O_3 \rightarrow CH_3SO + O_2 \qquad (12a)$$

The influence of reactions 2c and 12a is difficult to estimate because of the high uncertainty on the branching ratios k_{2c}/k_2 and k_{12a}/k_{12}. The value of k_{12a}/k_{12} has been estimated to be 15 $\pm$ 4% at ~1 Torr of He.[10] However, the yield of CH_3SO in reaction 12 may be higher at high pressure. In the present work, several experiments on the photolysis of DMDS/O_3/NO_2 mixture, where both CH_3S and CH_3SO radicals were generated in the reaction O + DMDS, showed that the SO_2 yield was close to unity, indicating either a high efficiency of CH_3S to CH_3SO conversion or a high yield of SO_2 in the reaction of CH_3S with O_3. Accounting for reaction 2c with $k_{2c}/k_2 = 13 \pm 6\%$[10] and assuming 100% conversion of CH_3S to SO_2 in the DMS/O_3/NO_2 mixture would result in an about 10% lower value of γ.

Atmospheric Implications

Results of this work on the SO_2 yield in the reactions of CH_3SO with NO_2 and O_3 are related to the question about efficiency of DMS to SO_2 conversion in the atmospheric oxidation mechanism of DMS. The oxidation pathway initiated by the H atom abstraction channel of the DMS reaction with OH and NO_3 is believed to proceed predominantly via CH_3S radical formation. If CH_3S is efficiently converted to CH_3SO, the SO_2 yield in the abstraction-initiated channel will depend on the fate of CH_3SO under atmospheric conditions. This fate in turn is determined by CH_3SO reactions with its main atmospheric oxidants O_2, NO_2, and O_3. The reaction of CH_3SO with O_2 has not been studied yet, and we assume here that it may be neglected compared to the reactions with O_3 and NO_2. For typical atmospheric concentrations, this assumption would require a rate constant value for the reaction $CH_3SO + O_2$ lower than about 10^{-20} cm^3 $molecule^{-1}$ s^{-1}. To some extent this assumption may be justified by analogy with the reaction $CH_3S + O_2$ which has been found to be very slow.[7] Then, neglecting the reaction with O_2, the efficiency of the abstraction pathway of DMS in the SO_2 production will be controlled by the efficiency of CH_3SO conversion to SO_2 by reactions of CH_3SO with NO_2 and O_3.

At low NO_x conditions of the remote marine troposphere, the potential climate effect of DMS due to aerosol production is considered to be the most important. With typical concentrations of O_3 and NO_2 of 30 ppbv and a few pptv, respectively, in such a region and with $k_2/k_1 = 2.13 \times 10^{-2}$ from this work the rate ratio of reactions $CH_3SO + O_3$ and $CH_3SO + NO_2$ will be higher than 100. Therefore, the reaction with O_3 will be the major path of CH_3SO oxidation and according to the results of this work the yield of SO_2 in the abstraction pathway will be close to 100%. That means also that CH_3SO_2 and CH_3SO_3 are not formed under these conditions and, consequently, low yield of methane sulfonic acid (MSA) is expected. Then, it may be concluded that SO_2 will be the H_2SO_4 precursor rather than SO_3, which may be formed from the CH_3SO_3 decomposition. The present results are in agreement with recent field measurements in the equatorial Pacific[32] where conversion of DMS to SO_2 was found to be 72 $\pm$ 22% and where the high-temperature H atom abstraction channel of DMS + OH reaction was predominant.

In polluted areas, the reaction of CH_3SO with NO_2 may become important. The rate ratio of reactions of CH_3SO with NO_2 and O_3 will be unity for 1 ppbv of NO_2 and 50 ppbv of O_3. In such a case, CH_3SO will be partly converted to CH_3SO_2. According to our results, the decomposition of CH_3SO_2 is slow, and it may react with O_3 and/or NO_2. The reaction with NO_2 is probably slow whereas the reaction with O_3 may lead to CH_3SO_3 and to MSA formation. Then, the relative yield of SO_2 and MSA in the abstraction channel of DMS oxidation would be dependent on the NO_2 concentration.

Acknowledgment. The authors gratefully acknowledge financial support of this work from the European Commission within the Environmental Program (EL CID project) and from the Région Centre and the STUDIUM program (research grant for D. Borissenko).

References and Notes

(1) Bates, T. S.; Lamb, B. K.; Guenther, A.; Dignon, J.; Stoiber, R. E. *J. Atmos. Chem.* **1992**, *14*, 315.

(2) Charlson, R. J.; Lovelock, J. E.; Andreae, M. O.; Warren, S. G. *Nature* **1987**, *326*, 655.

(3) Hynes, A. J.; Wine, P. H.; Semmes, D. H. *J. Phys. Chem.* **1986**, *90*, 4148.

(4) Williams, M. B.; Campuzano-Jost, P.; Bauer, D.; Hynes, A. J. *Chem. Phys. Lett.* **2001**, *344*, 61.

(5) Turnipseed, A. A.; Ravishankara, A. R. The Atmospheric Oxidation of Dimethyl Sulfide: Elementary Steps in a Complex Mechanism. In *Dimethylsulphide: Oceans, Atmosphere and Climate;* Restelli, G., Angeletti, G., Eds.; Kluwer Academic: Dordrecht, 1993; p 185.

(6) Ravishankara, A. R.; Rudich, Y.; Talukdar, R.; Barone, S. B. *Philos. Trans. R. Soc. London B* **1997**, *352*, 171.

(7) Tyndall, G. S.; Ravishankara, A. R. *J. Phys. Chem.* **1989**, *93*, 2426.

(8) Turnipseed, A. A.; Barone, S. B.; Ravishankara, A. R. *J. Phys. Chem.* **1992**, *96*, 7502.

(9) Tyndall, G. S.; Ravishankara, A. R. *J. Phys. Chem.* **1989**, *93*, 4707.

(10) Dominé, F.; Ravishankara, A. R.; Howard, C. J. *J. Phys. Chem.* **1992**, *96*, 2171.

(11) Turnipseed, A. A.; Barone, S. B.; Ravishankara, A. R. *J. Phys. Chem.* **1993**, *97*, 5926.

(12) Martinez, E.; Albaladejo, J.; Notario, A.; Jimenez, E. *Atm. Environ.* **2000**, *34*, 5295.

(13) Balla, R. J.; Nelson, H. H.; McDonald, J. R. *Chem. Phys.* **1986**, *109*, 101.

(14) Dominé, F.; Murrells, T. P.; Howard, C. J. *J. Phys. Chem.* **1990**, *94*, 5839.
(15) Martinez, E.; Albaladejo, J.; Aranda, A. *Chem. Phys. Lett.* **1999**, *308*, 37.
(16) Chang, P.-F.; Wang, T. T.; Lee, Y.-P. *J. Phys. Chem. A* **2000**, *104*, 5525.
(17) Kukui, A.; Bossoutrot, V.; Laverdet, G.; Le Bras, G. *J. Phys. Chem. A* **2000**, *104*, 935.
(18) Ray, A.; Vassalli, I.; Laverdet, G.; Le Bras, G. *J. Phys. Chem.* **1996**, *100*, 8895.
(19) Lee, E. K. C.; Loper, G. L. Electronic relaxation of small polyatomic molecules. In *Radiationless Transitions*; Lin, S. H., Ed.; Academic Press: New York, 1980; p 1.
(20) Okazaki, A.; Ebata, T.; Mikami, N. *J. Chem. Phys.* **1997**, *107*, 8752.
(21) Freeman, D. E.; Yoshino, Y. *Planet. Space Sci.* **1984**, *32*, 1125.
(22) Hearn, C. H.; Turcu, E.; Joens, A. *Atm. Environ.* **1990**, *24A*, 1939.
(23) Hynes, A. J.; Wine, P. H.; Nicovich, J. M. *J. Phys. Chem.* **1988**, *92*, 3846.
(24) DeMore, W. B.; Sander, S. P.; Golden, D. M.; Hampson, R. F.; Kurylo, M. J.; Howard, C. J.; Ravishankara, A. R.; Colb, C. E.; Molina, M. J. *JPL Publication 97-4;* Jet propalsion Laboratory, California Institute of Technology: Pasadena, CA, 1997.
(25) Atkinson, R.; Baulch, D. L.; Cox, R. A.; Hampson, R. F., Jr.; Kerr, J. A.; Rossi, M. J.; Troe, J. *J. Phys. Chem. Ref. Data* **1997**, *26*, 1329.
(26) Cooper, W. F.; Hershberger, J. F. *J. Phys. Chem.* **1992**, *96*, 5405.
(27) Clyne, M. A. A.; Whitefield, P. D. *J. Chem. Soc., Faraday Trans. 2* **1979**, *75*, 1327.
(28) Estupinan, E. G.; Nicovich, J. M.; Wine, P. H. *J. Phys. Chem. A* **2001**, *105*, 9697.
(29) Burkholder, J. B.; Ravishankara, A. R. *J. Phys. Chem. A* **2000**, *104*, 6752.
(30) Lee, J. H.; Tang, I. N. *J. Chem. Phys.* **1980**, *72*, 5718.
(31) Nip, W. S.; Singleton, D. L.; Cvetanovic, R. J.; Klemm, R. B. *J. Am. Chem. Soc.* **1981**, *103*, 3526.
(32) Davis, D.; Chen, G.; Bandy, A.; Thornton, D.; Eisele, F.; Mauldin, L.; Tanner, D.; Lenschow, D.; Fuelberg, H.; Huebert, B.; Heath, J.; Clarke, A.; Blake, D. *J. Geophys. Res.* **1999**, *104*, 5765.